

Linear and Nonlinear Properties of Pancharatnam's Phase in Polarization Optics

Hyrum Richardson

A senior thesis submitted to the faculty of
Brigham Young University
in partial fulfillment of the requirements for the degree of

Bachelor of Science

Surendra Singh, University of Arkansas and Michael Ware, Brigham Young University, Advisors

Department of Physics and Astronomy

Brigham Young University

April 2017

Copyright © 2017 Hyrum Richardson

All Rights Reserved

ABSTRACT

Linear and Nonlinear Properties of Pancharatnam's Phase in Polarization Optics

Hyrum Richardson
Department of Physics and Astronomy, BYU
Bachelor of Science

Pancharatnam's phase is the additional phase beyond the dynamical phase of electromagnetic radiation that arises due to polarization evolution, and although it is a fundamental property of polarization, the linear and nonlinear properties it exhibits are not well understood or discussed. A computer simulation extendable to any polarization circuit was developed that makes Pancharatnam's phase more intuitive and understandable. Two types of interferometers were tested, a symmetric Sagnac interferometer and a Mach-Zehnder interferometer, to measure the linearity and nonlinearity of Pancharatnam's phase. The simulation and experimental results were compared and shown to match closely. The linearity of Pancharatnam's phase can be predicted and measured, and our model is accurate to the physical phenomenon and useful for interferometry applications.

Keywords: Light Polarization, Pancharatnam's phase, Berry's Phase

Contents

Table of Contents	iii
List of Figures	iv
1 Introduction	1
1.1 Motivation	1
1.2 Background	2
1.3 Geometric Phase	6
1.4 Pancharatnam's phase	6
2 Computer Model	8
3 Methods and Materials	13
4 Results and Discussion	19
4.1 Linear Interferometer Data	19
4.2 Nonlinear Interferometer Data	21
4.3 Conclusion	23
Appendix A Source Code	24
A.1 Mathematica	24
A.2 Matlab	27
Bibliography	30
Index	31

List of Figures

1.1	Example Polarization	2
1.2	Poincaré Sphere	4
1.3	Example of Waveplate effect	5
1.4	Polarization Circuit and Pancharatnam's phase	7
2.1	Linear Circuit Example	9
2.2	Nonlinear Circuit Example	10
2.3	Nonlinear Angle Graph	11
2.4	Animation Stills	11
3.1	Mach-Zehnder Interferometers	13
3.2	Sagnac Interferometer and Model	15
3.3	Sagnac Interferometer and Model	16
3.4	Processing Example	17
3.5	Data Example	18
4.1	Linear Data	20
4.2	Nonlinear Data	21
4.3	Nonlinear Mach-Zehnder Data with simulation	22

Chapter 1

Introduction

1.1 Motivation

Pancharatnam's phase is a fundamental property of light polarization that is usually ignored in simple systems. Pancharatnam's Phase is a geometric phase shift that arises due to a change in polarization. This phase shift happens independently of the dynamical phase (spatial or temporal phase), so in systems where the optical path length changes, the geometric phase shift is not noticeable. However, Pancharatnam's Phase allows for phase control of fixed path length systems. As shown in this research, that control can have nonlinear characteristics, which is of particular interest in fast optical switching applications.

Pancharatnam's phase is not widely considered in optical theory and not often included in optics textbooks. In systems where optical path length changes or the change in polarization is not significant the effect from Pancharatnam's phase is not consequential enough to consider. This research seeks to expand understanding of the properties of Pancharatnam's phase, create an animation that makes the characteristics of the phase more intuitive, and compare our simulation to established models and experimental data.

The mechanics of Pancharatnam's phase will be discussed in detail in Section 1.2. Chapter 2 details the computer model that we built. Chapter 3 describes the interferometers constructed to measure Pancharatnam's phase, and Chapter 4 shows the results of our tests and establishes the validity of the computer model in predicting Pancharatnam's phase.

1.2 Background

Electromagnetic radiation oscillates in the plane perpendicular to the direction of propagation. The direction of that oscillation is the polarization of the light. The polarization can be represented in a few different methods which are important to our research. The general form for the electric field of light propagating in the z -direction is given by

$$\vec{E}(z,t) = (E_x\hat{x} + E_y e^{i\delta}\hat{y})e^{i\phi} \quad (1.1)$$

where δ represents the phase difference between the electric field's x and y components (E_x and E_y), and ϕ represents the dynamical phase as the wave propagates.

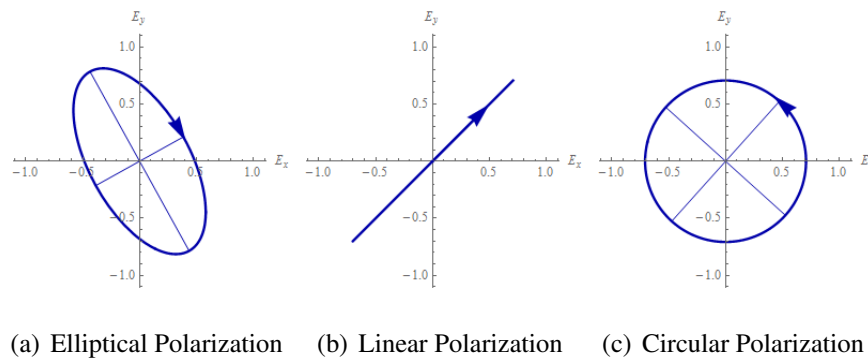


Figure 1.1 Three example polarization states.

The particular state of polarization depends on the relationship between the E_x , E_y and δ terms of the electric field equation. The general case for polarization is an ellipse as shown in Figure 1.1(a). Linear and circular polarization (Figure 1.1(b) and Figure 1.1(c)) can be considered

special cases of the general case. The angle between the major axis of the ellipse and the x or y axis is determined by

$$\frac{1}{2} \tan^{-1} \left(\frac{2E_x E_y \cos \delta}{E_x^2 - E_y^2} \right) \quad (1.2)$$

The minor axis is always 90° from the major axis. The ellipticity is then determined by the ratio between the minor and major axes. The special cases occur when the ellipticity factor is 0, corresponding to linear polarization ($\delta = 0, \pi$) or 1, corresponding to circular polarization ($\delta = \pi/2$).

The polarization state can also be represented by the normalized Jones vector

$$\begin{pmatrix} E_x \\ E_y e^{i\delta} \end{pmatrix} \quad (1.3)$$

with the terms representing \hat{x} and \hat{y} components from Equation 1.1. Any change in polarization can be represented by a Jones matrix operating on the polarization state vector.

A waveplate is an optical device constructed out of a birefringent material that alters the polarization. The difference in index of refraction depending on incident polarization (birefringence) creates a phase shift between horizontal and vertical components of the electric field. The overall change in polarization depends on the angle between the optical axis, the orientation that has a lower index of refraction. A waveplate can be generalized in the Jones matrix notation

$$M_\xi(\theta) = \begin{pmatrix} \cos^2 \theta + e^{i\xi} \sin^2 \theta & \sin \theta \cos \theta - e^{i\xi} \sin \theta \cos \theta \\ \sin \theta \cos \theta - e^{i\xi} \sin \theta \cos \theta & \sin^2 \theta + e^{i\xi} \cos^2 \theta \end{pmatrix} \quad (1.4)$$

where ξ represents the phase shift between the fast and slow axes of the waveplate. Quarter-wave plates ($\xi = \pi/2$) and half-wave plates ($\xi = \pi$) are commonly used in optical systems to alter polarization. Linear polarizers, which use absorption rather than birefringence, can use the same matrix when $\xi = 0$. The effect from multiple optical devices can be computed by multiplying the matrices representing them in reverse order. We use this method in Section 1.4 to show the existence of Pancharatnam's phase.

A more visual way of representing polarization is on a Poincaré sphere, a useful graphical tool for mapping unique polarization states and geometrical phase. The Poincaré sphere is an abstract space where each point on a unit sphere represents a unique polarization state. A paper from Vyas establishes the connection between Stoke's parameters and a spherical interpretation of a polarization space. [1] The polarization orientation and ellipticity are represented as points on the surface of the sphere. The poles represent left-handed circularly polarized light (LCP) and right-handed circularly polarized light (RCP) in Figure 1.2, and the equator represents linear polarization at any angle. Any other point is an elliptical polarization state. Any two antipodal (directly opposite) points are orthogonal and won't interfere.

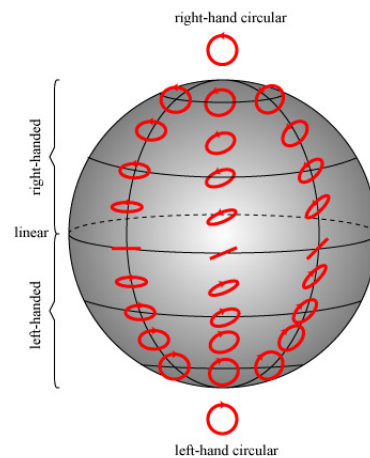


Figure 1.2 Poincaré Sphere (Image Source: goo.gl/Hb1mnk)

The Poincaré sphere gives us a three-dimensional space to visually represent any change in polarization. As an example, RCP light passes through a quarter-wave plate with fast-axis $\frac{\pi}{2}$ from horizontal which is represented by pt. A in Figure 1.3. By Jones matrices, we can compute the resultant polarization:

$$\frac{1}{\sqrt{2}} M_{\pi/2}(\pi/2) \begin{pmatrix} 1 \\ i \end{pmatrix} = \frac{i}{\sqrt{2}} \begin{pmatrix} 1 \\ 1 \end{pmatrix} \quad (1.5)$$

The light after the waveplate is linearly polarized 45° from horizontal (equal parts horizontal and

vertical). The $\frac{i}{\sqrt{2}}$ term in 1.5 is unimportant to the overall polarization. This process can be represented on a Poincaré sphere as the great arc between the two polarization points represented as the arc between pt. A and pt. B in Figure 1.3. The arc associated with a waveplate depends on the phase properties of the waveplate (ξ) and the angle between the fast axis and the electric field of the incident light (θ). The orientation of the polarization change (great arc) depends on the angle θ .

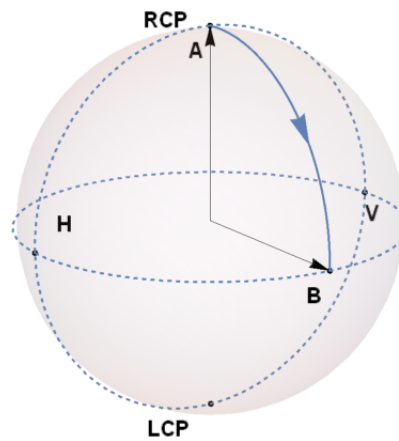


Figure 1.3 Example of Waveplate effect

1.3 Geometric Phase

In a 1988 paper titled "The Geometric Phase", Physicist Sir Michael Berry discussed the general properties of geometric phase. [2] A simple example of geometric phase is a Foucault pendulum. The pendulum oscillates as earth rotates around it, and its rotation from the plane of its original oscillation is determined by its path around the axis of rotation. After one whole cycle (24 hours), the total geometric phase shift is 360° for a pendulum at the poles, 0° at the equator, and some other angle for any point in between.

Geometric phase is present in a number of systems involving a cyclic adiabatic process. When these principles are applied to optical systems, the geometric phase is called Pancharatnam's phase.

1.4 Pancharatnam's phase

In 1956, S. Pancharatnam showed that a geometric phase separate from the dynamical phase arises when an electromagnetic wave undergoes a polarization circuit. [3] Here we define a polarization circuit as the cyclic evolution (change) of polarization that begins and ends at the same polarization state. Figure 1.4 gives an example of a polarization circuit. Note that the solid angle enclosed by path ABCA is equal to that enclosed by ACBA. In other words, the direction of the polarization circuit is arbitrary.

By Pancharatnam's theorem [3], the phase shift given a polarization circuit is

$$\gamma = -\frac{1}{2}\Omega(A, B, C) \quad (1.6)$$

where $\Omega(A, B, C)$ is the solid angle of the spherical triangle (spherical excess) enclosed by points A, B, and C on the Poincaré sphere (Figure 1.4). [4] We will use γ to represent Pancharatnam's phase in our figures. It is proportional to the solid angle Ω (area on the surface of the sphere enclosed by the great arcs between polarization states). When the electromagnetic wave makes a

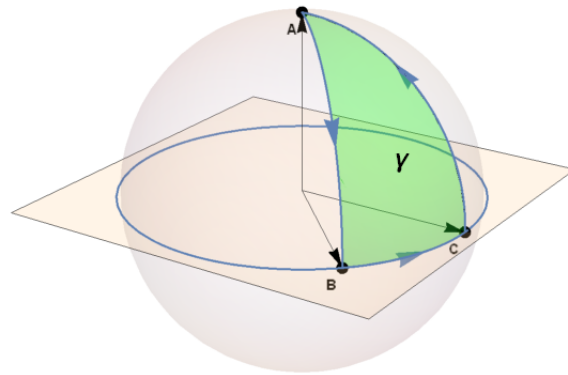


Figure 1.4 Example of a polarization circuit on a Poincaré sphere (A, B, and C represent three distinct polarization states)

complete circuit, the geometrical phase shift is equal to solid angle enclosed by the polarization circuit. We will use this geometric interpretation of Pancharatnam's phase to build an intuitive model for Pancharatnam's phase. [4]

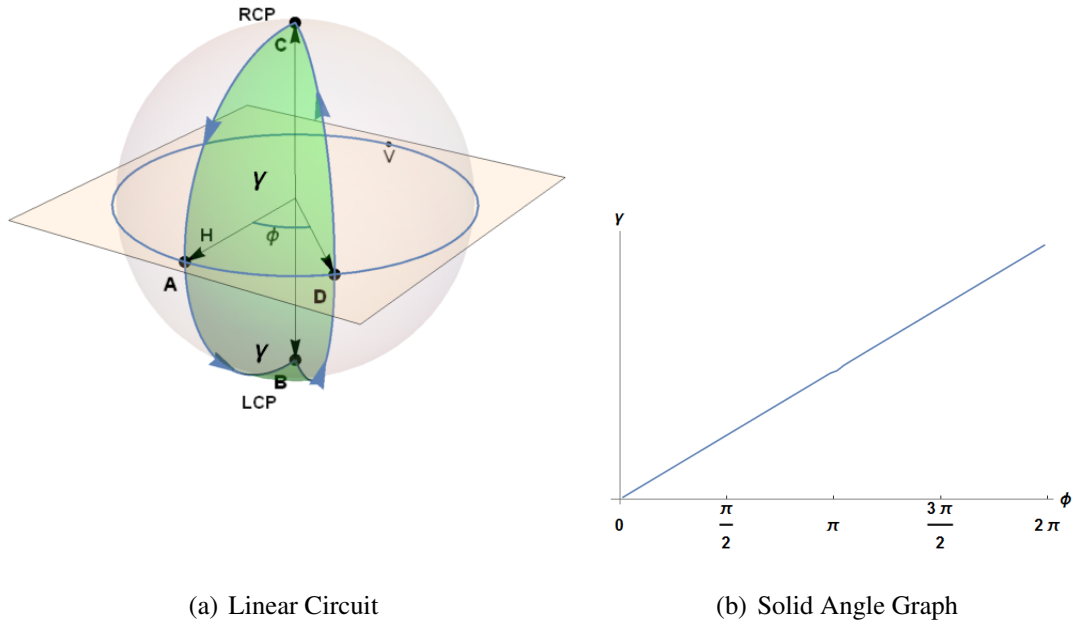
Chapter 2

Computer Model

One focus of this research is to build a geometric model of Pancharatnam's phase that could simulate any polarization circuit. By using a Poincaré sphere, the properties of Pancharatnam's phase can be made more intuitive and visual. As discussed in Ch. 1, the solid angle between three polarization states mapped onto a unit sphere represents the geometric phase shift of a beam of light passing through those polarizations. In this chapter, we discuss the construction of a visual computer simulation and its predictions.

Mathematica was used to build the working geometric model of a polarization circuit. The three polarization states are placed on a unit sphere with vectors pointing from the origin to each point. The cross product of a pair of two vectors defines a plane that contains the two vectors and the great circle between them. The intersection between the space enclosed by three planes (defined by three permutative pairs of vectors), and the surface of the sphere gives the solid angle. This area represents Pancharatnam's phase γ (Figure 1.4).

By changing the position of one of the points, the enclosed solid angle will change. The properties of Pancharatnam's phase can be easily observed by the solid angle on the sphere. The solid angle's (γ) rate of change will depend on how the polarization circuit changes. Changing the position of a point represents the rotation of a polarizer or waveplate. For clarity, the great circles



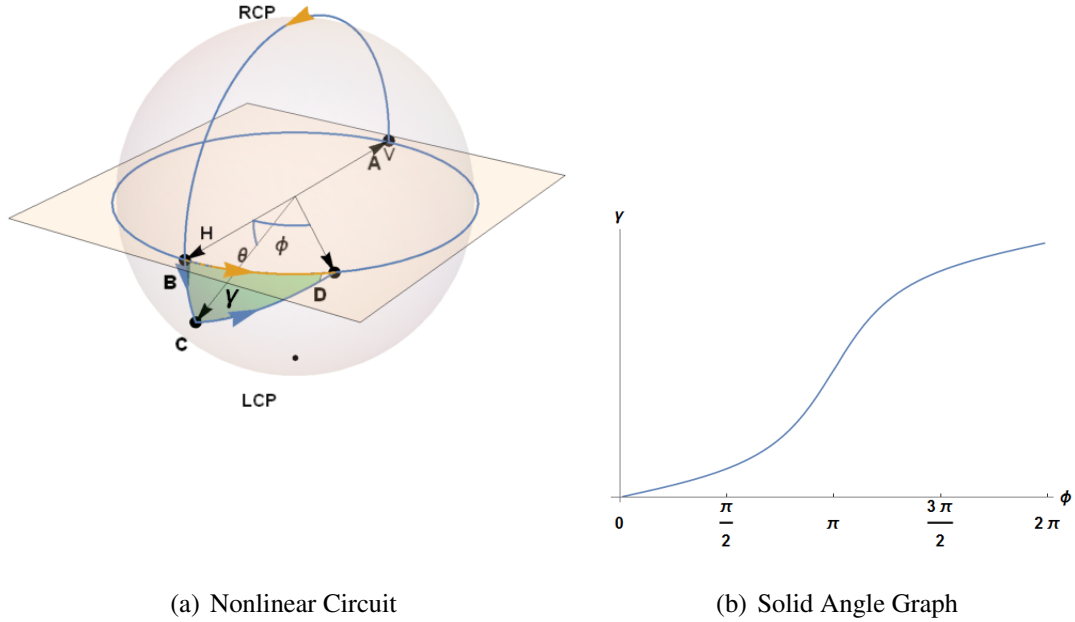
(a) Linear Circuit

(b) Solid Angle Graph

Figure 2.1 Example of linear polarization circuit. (a) Linear circuit represented on Poincaré sphere. Angle ϕ increases as pt. D moves counterclockwise (as viewed from above). (b) Graph of the solid angle's dependence on ϕ .

(or great arcs) between each point have been included, along with arrows indicating the direction of the polarization change (e.g. between pt. C and pt. A in Figure 2.1(a)). It should be noted again that the direction of the change is arbitrary as the area enclosed doesn't change. The two polarization circuits that were experimentally observed in Chapter 3 are here modeled and simulated to predict the properties of Pancharatnam's phase.

First, a linear polarization circuit was modeled (Figure 2.1(a)). A linearly polarized beam (point A) passes through a quarter-wave plate with fast-axis 45° from vertical (pt. A to pt. B), then through a half-wave plate (pt. B to pt. C) at angle ϕ from vertical. Finally, another quarter-wave plate with fast-axis 45° from vertical (the opposite direction) returns the polarization to the original polarization (pt. C to pt. A) (also see Figure 3.1(a)). As the half-wave plate is rotated, pt. D moves around the equator. As pt. D moves (ϕ increases), the solid angle γ increases with linear



(a) Nonlinear Circuit

(b) Solid Angle Graph

Figure 2.2 Example of nonlinear polarization circuit. (a) Linear circuit represented on Poincaré sphere. Angle ϕ increases as pt. D moves counterclockwise (as viewed from above). Nonlinearity depends on angle θ . (b) Graph of the solid angle's dependence on ϕ .

dependence on ϕ (Figure 2.1(b)) [5].

The results of this model match the Jones matrix prediction of the same polarization circuit.

($M_{\pi/2}$ represents a quarter-wave plate and M_{π} represents a half-wave plate)

$$M_{\pi/2}(\pi/4)M_{\pi}(\phi)M_{\pi/2}(-\pi/4) \begin{pmatrix} 1 \\ 0 \end{pmatrix} = \begin{pmatrix} e^{2i\phi} \\ 0 \end{pmatrix} \quad (2.1)$$

The phase shift of the resultant wave compared to the incident wave is Pancharatnam's phase γ .

The Jones matrix prediction shows that $\gamma \propto \phi$ which matches our computer model in Figure 2.1(b).

Next, an example of a nonlinear polarization circuit was modeled (Figure 2.2(a)). A linearly polarized beam is split by a beam splitter. Half of the beam passes through a half-wave plate with fast-axis 45° from normal (pt. A to pt. B). The other beam passes through a half-wave plate with

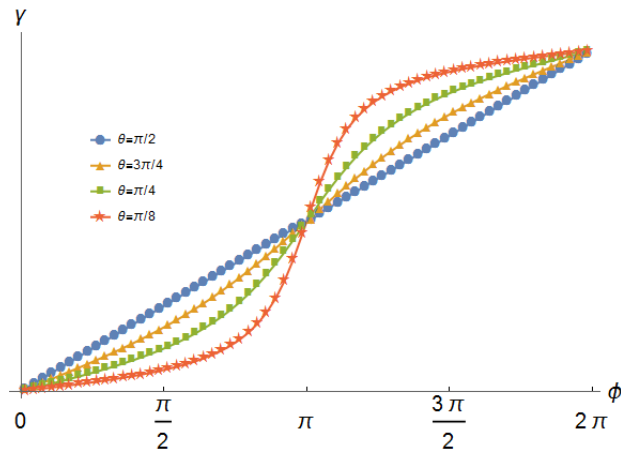


Figure 2.3 Graph of nonlinear Pancharatnam's phase with values of θ (see Figure 2.2(a))

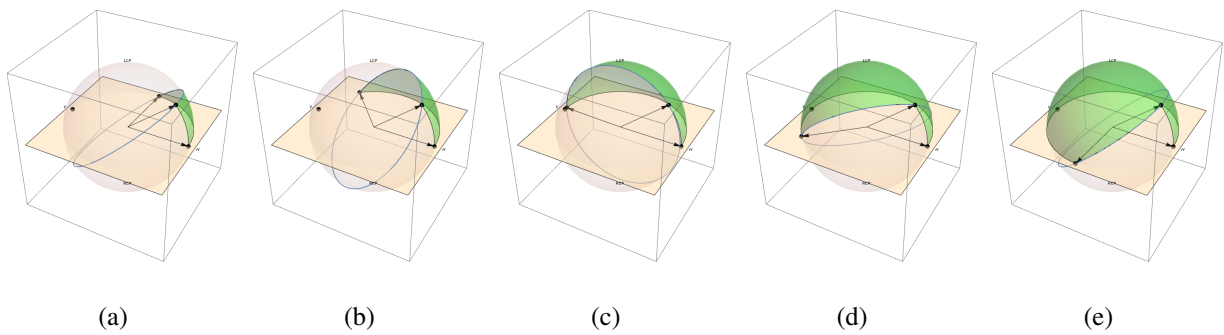


Figure 2.4 Stills from animation for $\theta = \frac{\pi}{8}$ from the attached .gif [6]

fast-axis 45° from normal tuned to a different wavelength than the beam (for example a 808 nm half-wave plate for a 633 nm beam). This causes the polarization to overshoot or undershoot the equator (pt. A to pt. C). The beams are recombined and passed through a rotating linear polarizer (pt. B to pt. D and pt. C to pt. D)(also see Figure 3.1(b)). As pt. D moves (ϕ increases), γ increases as shown in Figure 2.2(b). Note that if ϕ is decreasing instead of increasing, the direction of the change in area is simply reversed, but the properties are effectively the same.

In the nonlinear circuit, the angle θ ($\angle BC$ in 2.2(a)) has a significant effect on the properties of the phase shift. If θ increases to $\frac{\pi}{2}$, then the phase shift is the same as the linear circuit shown in Figure 2.1(a). As θ decreases, the nonlinear effect is more pronounced (Figure 2.3).

The animation of this process makes the nonlinear nature of Pancharatnam's phase more apparent and intuitive. Figure 2.4 shows a few stills of the animation. The stills shown are evenly spaced in time. The rapid increase in area from Figure 2.4(b) to Figure 2.4(d) coincides with the steep slope of the $\frac{\pi}{2}$ to $\frac{3\pi}{2}$ range in 2.3. A link to a GIF of the animation has been included with this paper. [6]

Our geometric model matches theoretical findings of other papers using a slightly different methodology. [4, 7] Our model was intended to be more visual than others, but it nonetheless agrees with other predictions.

Chapter 3

Methods and Materials

This chapter discusses the experimental methods we used to determine our model's accuracy and usefulness. We constructed a Mach-Zehnder and Sagnac interferometer, and tested each with a linear and nonlinear polarization circuit. A Helium-Neon laser at of 633nm was the primary laser for testing. All data is from the He-Ne 633nm laser except where indicated. First we describe the Mach-Zehnder interferometer, with a linear and nonlinear polarization circuit. Then we describe the Sagnac interferometer, with a linear and nonlinear polarization circuit.

The Mach-Zehnder interferometer allowed for the most customization of polarization path. In the linear Mach-Zehnder case (Figure 3.1(a)), only one path changed polarization. Path A's

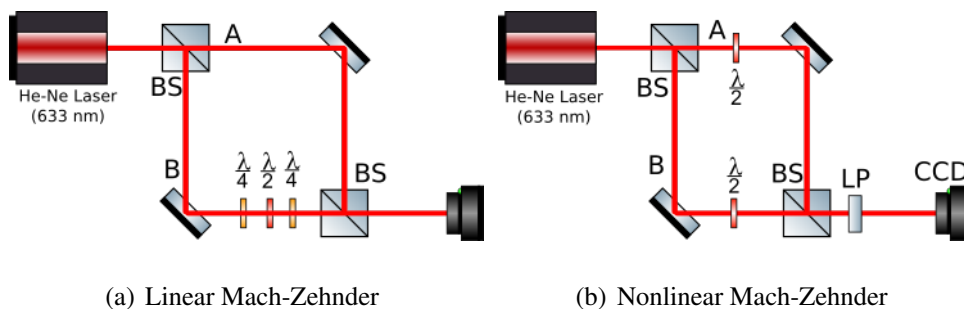


Figure 3.1 Mach-Zehnder Interferometers (BS = Beam Splitter, $\frac{\lambda}{2}$ = Half-wave plate, $\frac{\lambda}{4}$ = Quarter-wave plate)

polarization is unchanged. Path B passes through a quarter-wave plate with fast-axis 45° from vertical, then through a half-wave plate on a rotating motor. Finally, it passes another quarter-wave plate with fast-axis 45° from vertical (the opposite direction). The two paths are recombined, then observed on a CCD.

The nonlinear Mach-Zehnder case requires both paths to change polarization and utilizes two different kinds of half-wave plates. In the nonlinear Mach-Zehnder case (Figure 3.1(b)), Path A passes through a half-wave plate tuned to 633nm. Path B passes through a half-wave plate designed for 808nm, making the polarization elliptical. Then both passed through the same linear polarizer to allow the two paths to interfere, then the pattern was observed on a CCD. The angle θ (see Figure 2.2(a) between the resulting polarization of path B after the 808nm half-wave plate and the linear polarization plane (equator) of the Poincaré sphere is found by calculating the effect of the waveplate for an incident wavelength different from the wavelength for which it was designed. The waveplate's phase effect on the polarization is described by the equation:

$$\Delta\phi = \frac{2\pi}{\lambda}\Delta nd \quad (3.1)$$

where $\Delta\phi$ is the resultant phase shift, Δn is the difference between the fast- and slow-axis's indices of refraction, and d is the width of the wave-plate. [8] $\Delta\phi$ is set to π for a waveplate. Solving for Δnd and substituting Δnd into the equation again for a wavelength of 633nm and solving for $\Delta\phi$ gives:

$$\Delta\phi = \frac{2\pi}{633nm} \frac{808nm}{2} = \frac{808}{633}\pi \quad (3.2)$$

Equation (3.2) refers to the total polarization shift which overshoots the linear polarization equator. We define θ as the angle between the plane and the point which is:

$$\theta = \Delta\phi - \pi = \left(\frac{808}{633} - 1\right)\pi \approx 0.87rad \quad (3.3)$$

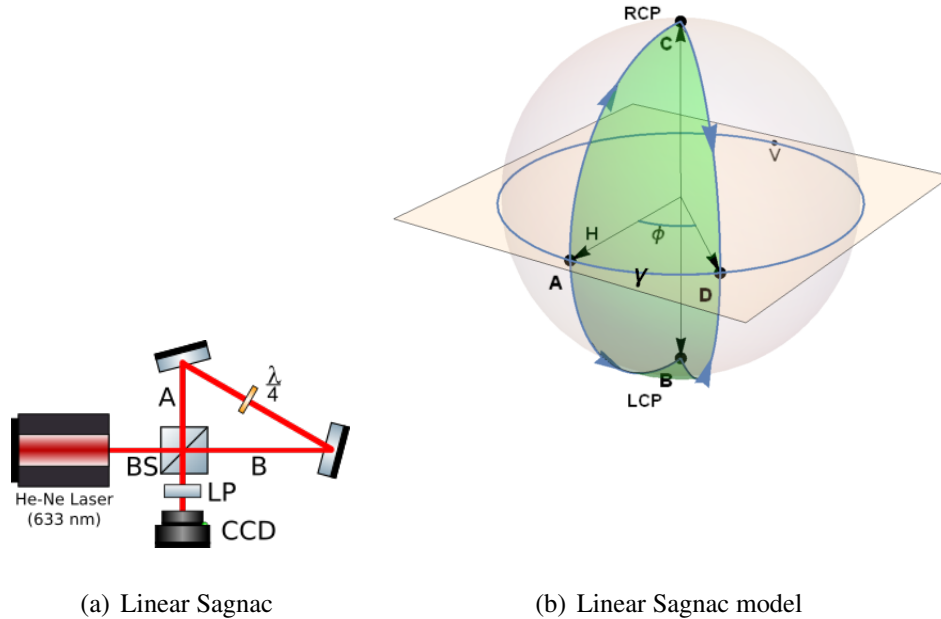


Figure 3.2 Sagnac interferometer and model (BS = Beam Splitter, $\frac{\lambda}{2}$ = Half-wave plate, A = Path A, B = Path B)

This angle θ determines the nonlinearity of Pancharatnam's phase as the linear polarizer in Figure 3.1(b) rotates.

The Sagnac interferometers (Figure 3.3(a)) proved more stable for accurate measurements. In the linear Sagnac interferometer, both beams pass through the same quarter-wave plate oriented 45° from vertical but in opposite directions. One path is pt. A to pt. B in Figure 3.2(b) (to LCP pole) and the other is pt. A to pt. C (to RCP pole). Then both paths are brought to the same polarization at pt. D and observed on a CCD camera. Pancharatnam's phase γ has the same characteristics as the linear Mach-Zehnder interferometer.

In the nonlinear setup, both paths of 633nm light pass through a half-wave plate designed for 808nm (with polarization shift defined in 3.2 above), but in opposite directions. One path is pt. A to pt. B in Figure 3.3(b)(passing through the RCP pole) and the other is Pt. A to Pt. C (passing

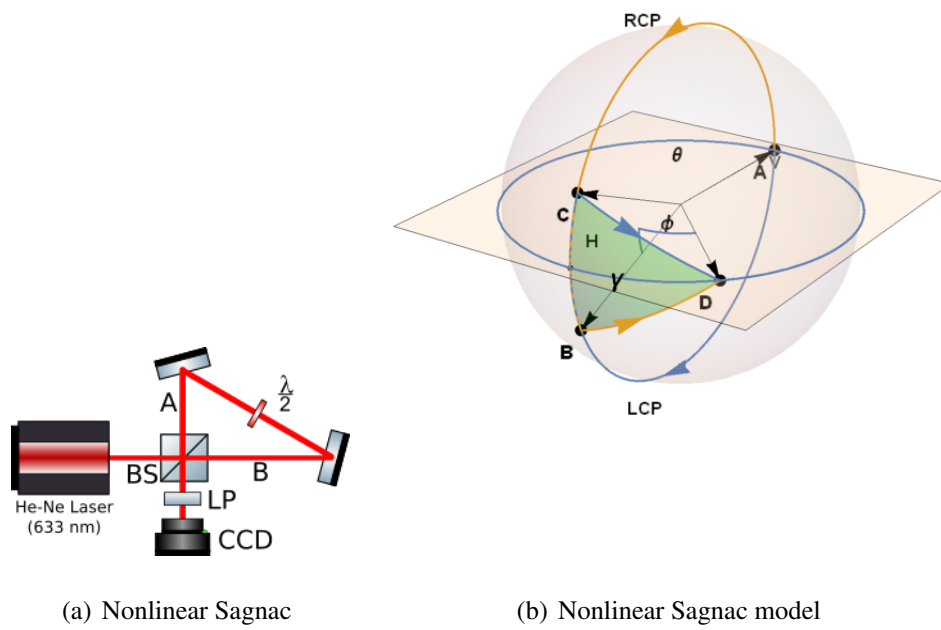


Figure 3.3 Sagnac interferometer and model (BS = Beam Splitter, $\frac{\lambda}{2}$ = Half-wave plate, A = Path A, B = Path B)

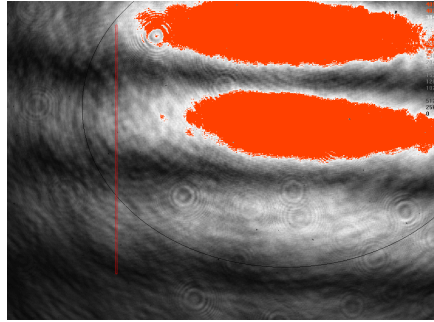
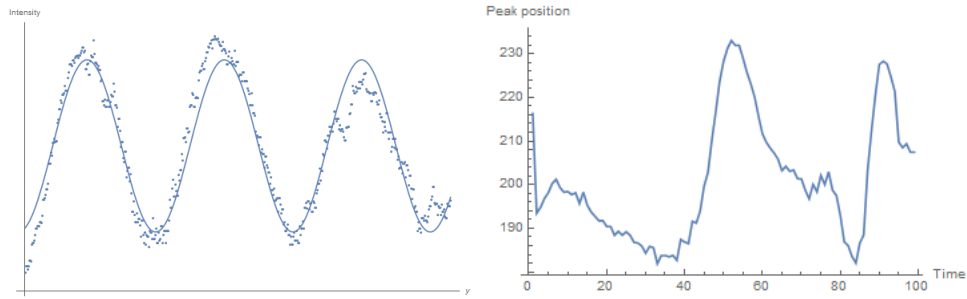


Figure 3.4 Example of Bitmap processing procedure

through the LCP pole). Then both paths are brought to the same polarization at pt. D and observed on a CCD camera. The solid angle γ is simply twice that of Figure 2.2(a) for the same angle θ . The same nonlinear characteristics are present.

The data from each of these interferometers is presented in 4, but due to software and other limitations described below, we needed a unique method of determined the characteristics of the phase shift for each interferometer. The software associated with the camera used to detect interference patterns produced bitmap frames of the pattern. Although the interference pattern shift is visible, a way to measure the phase shift numerically was needed. One of the greatest difficulties in the measurement process was the change in intensity as the analyzer rotated. As angle ϕ reaches π (refer to Figure 3.3(b)), Pt. D and Pt. B become antipodal and the intensity from that arm of the interferometer goes to zero. We saturated our camera by increasing the total intensity of the laser in order to get as much data as possible when the intensity dropped.

A unique data processing procedure that could extrapolate the phase from a changing intensity interference pattern was needed. Each frame of the interference pattern was run through a custom built program that took a pixel brightness measurement (analogous to intensity) at the same set of pixels for each picture in the series. We selected the area indicated by the red line in Figure 3.4 to measure on each frame. The line is four pixels wide, and the average of the two horizontal pixels inside the line was associated with a vertical pixel coordinate. By lining up the vertical placement



(a) Data points with cosine wave regression (b) Peak position vs time graph (arb. units)

Figure 3.5

along the x-axis of a new graph, a view of the interference waveform can be seen (Figure 3.5(a)).

A general cosine function is defined

$$f(x) = a + b \cos(kx - d) \quad (3.4)$$

with a , b , and d dependent and with k fixed. Wavenumber k was set equal to the mean of the wavenumbers of the cosine wave in a few example frames. This fits a cosine wave close to the data points for each frame, but maintains the same period between frames. This assumption was made because the path length and alignment of the setup is unchanged, and so the period of the interference pattern remains unchanged. (see A.2 for the Matlab code used for this process)

The y-coordinate of each peak was recorded for each frame. The result is a peak coordinate vs. polarizer angle as the polarizer in the optical setup rotates. The movement of the peak is directly related to the phase shift from Pancharatnam's phase. Figure 3.5(b) shows an example of one of these graphs that was acquired during the testing process. This particular graph is not meaningful, but it illustrates clearly what the graph represents. It graphs the position of one particular intensity peak, the one that starts at 215 pixels down the red line in Figure 3.4. As time progressed (polarizer rotated), the peak shifted up to about pixel 150 and then down to 230 and so on.

Chapter 4

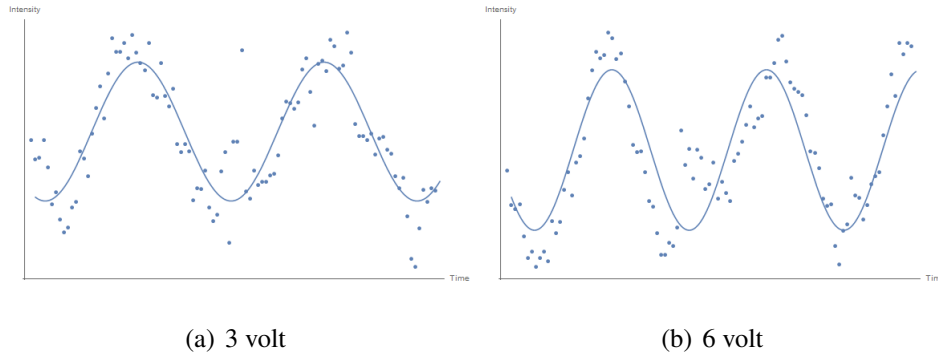
Results and Discussion

In this chapter, we discuss the results of the interferometer measurements and their significance. First, we discuss the linear measurements that served as a proof of concept for our measurement system and Pancharatnam's phase. Then we discuss the data from the nonlinear interferometers. Finally, we compare these results with our simulation and discuss the implications of our research.

4.1 Linear Interferometer Data

The first tests were used to verify the existence of Pancharatnam's phase and check the accuracy of our data analysis procedure. The first tests were done using an Argon-Ion laser with the linear Mach-Zehnder interferometer and 514nm waveplates to match the laser (Figure 3.1(a)). The intensity was measured at particular points for different waveplate rotation speeds.

The data collected was fit to a cosine wave regression. Figure 4.1(a) shows the data collected as the rotating motor ran with 3 V while Figure 4.1(b) shows the data with 6 V to the motor. The graph shows the intensity at a single point on a time graph. Note that time is analogous to the angle of the waveplate in the motor ϕ . The 3 V and 6 V data have different periods, which is to be expected because the waveplate is rotating faster with a larger voltage across the motor. Table 4.1

**Figure 4.1**

shows the three different speeds that were tested and the measured results.

Table 4.1 Linear Interferometer Results: Column 1 refers to the voltage across the motor turning the waveplate. Column 2 is the observed period of the motor divided by 2 (as the observed period for a half rotation of the half-wave plate is equivalent to one rotation on the Poincare sphere). Column 3 is the period measured by CCD (see Figure 4.1). Column 4 is the percent error between the theoretical and experimental values.

Voltage	Waveplate period (s)	Measured period (s)	% error
3	6	5.81	3.17
6	2.4	2.59	7.92
8	1.7	1.42	16.47

Much of the error in these measurements was attributed to inconsistency in the power supply of the Argon-Ion laser. In both Figures 4.1(a) and 4.1(b), many of the data points are far from the cosine function. This leads to a lower accuracy in our measured period numbers in 4.1. Nevertheless, this data verifies the existence of Pancharatnam's phase. We have shown in our computer simulation 2.1(b) that the phase shift is directly related to the angle of polarizer. This matches our interferometry data. A linear relationship between polarizer angle and phase shift will give a sine function of intensity at any given point.

4.2 Nonlinear Interferometer Data

The best data for the nonlinear case of Pancharatnam's phase came from the nonlinear Mach-Zehnder interferometer (Figure 3.1(b)). Figure 4.2(a) presents an important characteristic of Pancharatnam's phase. This data shows the position of a single peak through two full cycles of the polarizer, demonstrating the characteristic that Pancharatnam's phase continues to build rather than cycling back to zero. A comparison between the theoretical model (Figure 3.3(b)) and the experimental data (Figure 4.2(a)) is shown in Figure 4.2. This graph isolates a single period of the polarizer and shows the closeness of our model to the actual phenomenon despite the noise in the experimental data.

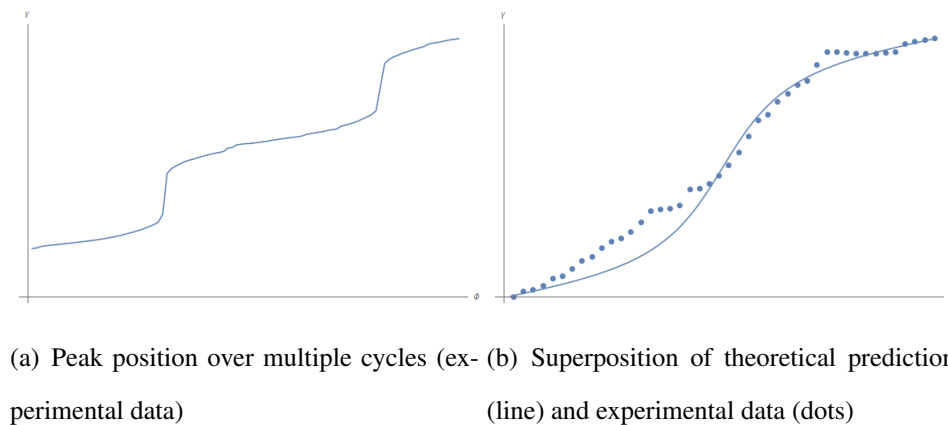


Figure 4.2 Data from Nonlinear Mach-Zehnder interferometer

By observing the position of all of the interference pattern peaks, we can get a better idea of the accuracy of our model. This is shown in Figure 4.3. Each vertical line of four dots represents a single frame from the camera, and each dot represents the position of an intensity peak of the interference pattern. In the data, some inconsistency of image collection procedure is apparent. We measured the actual rotation of the analyzer and we found that while it is close to the repeating period of the data, it doesn't match due to the fluctuations discussed. We found that the framerate of our image acquisition software fluctuated over the course of data collection. For example, it would

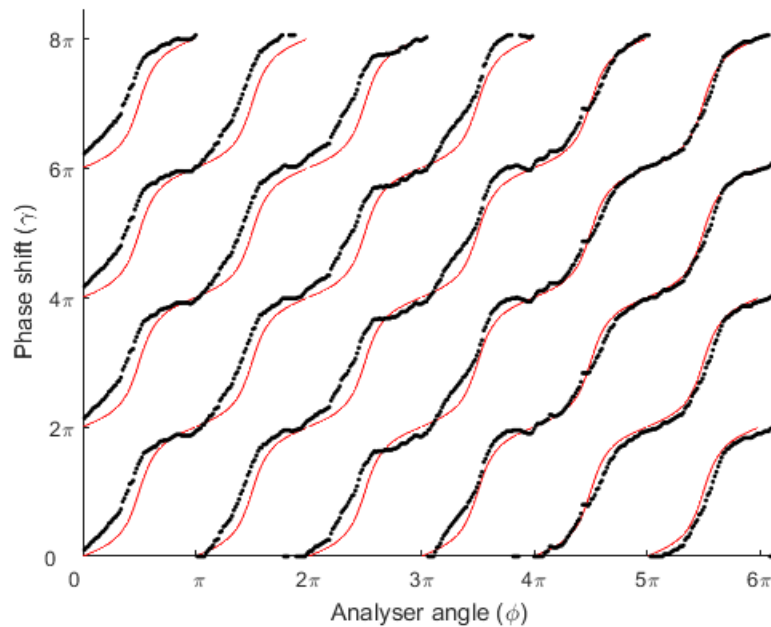


Figure 4.3 Experimental data (black dots) compared with simulation (red line)

record from 6-8 frames per second depending on the computer speed with which it could save the images. The linear case demonstrated that the pattern should oscillate strictly periodically, so we should expect that a constant polarizer speed should give us a periodic pattern. To more accurately measure the validity of our model, in this graph we scaled and repeated the simulation line according to the average period of the data to eliminate error from our image system.

The data from the interferometer matches the simulation well. Many of the fluctuations in the interferometer data are repeated vertically which we can attribute to error in our image collection system. For example, between 2π and 3π , the experimental data dips below the prediction, but the same dip is repeated vertically for all 4 peaks in the interference pattern. This indicates to us that the error was caused by the image acquisition system (perhaps the framerate sped up during that time) or a vibration in the table which would effect the whole interference pattern.

Despite these inconsistencies, many parts of our data match the prediction made by our simulation very well. From 0 to π in Figure 4.3 demonstrates the accuracy of our model.

4.3 Conclusion

These experiments verified previous measurements of Pancharatnam's phase, in both the linear and nonlinear cases. A geometric simulation of Pancharatnam's phase that can apply to any arbitrary circuit was created and shown to predict well the nonlinearity of the phase change. The data collected is consistent with the theory presented.

The simulation that we created provides a visual for Pancharatnam's phase that builds intuition and increases understanding of this important phenomenon. We found that this model is useful for predicting phase changes of any kind of polarization circuit, even those with characteristics that are less predictable. The novel method of detecting the phase variation using peak intensities from a cosine curve fit has important implications and can be reused in future research.

Pancharatnam's phase exists in any system that changes polarization. A better understanding of its properties can improve interferometry research by allowing researchers to monitor and control phase in ways besides changing path length. We hope this research can be continued by further investigating these properties and will contribute to an ever improving understanding of light.

Appendix A

Source Code

A.1 Mathematica

The code for creating the nonlinear animation as described in Section 2 and cited as [6].

```
1 Clear["`*"]
2 SetDirectory[NotebookDirectory[]];
3 j = \[Pi] (808/633 - 1);
4 q1 = {Sin\[Pi]/2 Cos[0], Sin\[Pi]/2 Sin[0],
5   Cos\[Pi]/2}; q2 = {Sin[j] Cos[0], Sin[j] Sin[0], Cos[j]};
6 q3[k_] = {Sin\[Pi]/2 Cos[k], Sin\[Pi]/2 Sin[k], Cos\[Pi]/2};
7
8 o = {0, 0, 0};
9
10 list2 = Table[{k,
11   RegionMeasure[
12     DiscretizeRegion [
13       ImplicitRegion [
14         x^2 + y^2 + z^2 == 1 &&
15         If [k < \[Pi], {x, y, z}.Cross[q1, q2] <
```

```

16      0 && {x, y, z}.Cross[q1, q3[k]] >
17      0 && {x, y, z}.Cross[q2, q3[k]] < 0,
18      y > 0 &&
19      z > 0 || {x, y, z}.Cross[q1, q2] >
20      0 && {x, y, z}.Cross[q1, q3[k]] <
21      0 && {x, y, z}.Cross[q2, q3[k]] < 0], {x, y,
22      z}}], {k, \[Pi]/64, 2 \[Pi] - \[Pi]/64, \[Pi]/32};
23
24 PoincareSphere2 =
25   Graphics3D[{Opacity[0.1],
26     Sphere[{0, 0, 0}, 0.98], {Opacity [0.5],
27     Polygon[{{-1.1, -1.1, 0}, {1.1, -1.1, 0}, {1.1, 1.1, 0}, {-1.1,
28     1.1, 0}}]}, ImageSize -> Large];
29 StoC[{r_, \[Theta]_, \[Phi]_} := {r Sin[\[Theta]] Cos[\[Phi]],
30   r Sin[\[Theta]] Sin[\[Phi]], r Cos[\[Theta]]};
31 greatcircle2 [{\[Theta]1_, \[Phi]1_}, {\[Theta]2_, \[Phi]2_} :=
32   Module[{}, c = StoC[{1, \[Theta]1, \[Phi]1}];
33   d = StoC[{1, \[Theta]2, \[Phi]2}];
34   q = Normalize[d - Dot[d, c]/Dot[c, c] c];
35   ParametricPlot3D[Cos[w] c + Sin[w] q, {w, 0, 2 Pi}]]
36 point[\[Theta]_, \[Phi]_] =
37   Point[{Sin[\[Theta]] Cos[\[Phi]], Sin[\[Theta]] Sin[\[Phi]],
38     Cos[\[Theta]]}];
39 points2 =
40   Graphics3D[{PointSize[.02], {point[j, 0], point[\[Pi]/2, 0],
41     point[\[Pi]/2, k], point[\[Pi]/2, \[Pi]]}}];
42 labels2 =
43   Graphics3D[{Text[H, {1.15, 0, 0}], Text[V, {-1.15, 0, 0}],
44     Text[LCP, {0, 0, 1.15}], Text[RCP, {0, 0, -1.15}]}];
45 arrows2 =

```

```

46 Graphics3D[{Thickness[Small], Arrowheads[Large],
47   Arrow[{o, #}]}] & /@ {q1, q2, q3[k]};
48
49 pics2 = Table[
50   Show[PoincareSphere2, points2, labels2, arrows2,
51     greatcircle2[{j, 0}, {\[Pi]/2, k}],
52     ContourPlot3D[
53       x^2 + y^2 + z^2 == 1, {x, -1, 1}, {y, -1, 1}, {z, -1, 1},
54       ContourStyle -> {Opacity[0.3], Green},
55       RegionFunction ->
56         Function[{x, y, z},
57           If[k < \[Pi], {x, y, z}.Cross[q1, q2] <
58             0 && {x, y, z}.Cross[q1, q3[k]] >
59             0 && {x, y, z}.Cross[q2, q3[k]] < 0,
60             y > 0 &&
61             z > 0 || {x, y, z}.Cross[q1, q2] >
62             0 && {x, y, z}.Cross[q1, q3[k]] <
63             0 && {x, y, z}.Cross[q2, q3[k]] < 0}],
64       Mesh -> None]], {k, \[Pi]/64, 2 \[Pi] - \[Pi]/64, \[Pi]/32}];
65 Export["PancharatnamFinalNL.gif",
66   Table[{Show[pics2[[i ]]],
67     Show[ListLinePlot[list2, ImageSize -> Large],
68     Graphics[{PointSize[Large], Red, Point[{list2[[i ]]}]}]}, {i, 1,
69     64, 1}]];
70 Manipulate[{Show[pics2[[i ]]],
71   Show[ListLinePlot[list2, ImageSize -> Large],
72   Graphics[{PointSize[Large], Red, Point[{list2[[i ]]}]}]}, {i, 1,
73   64, 1}]

```

A.2 Matlab

The code for Matlab analysis program referred to in Section 3.

```
1 clear ;
2 close all ;
3
4 temp = xlsread('.\MZN1data.csv');
5 d=flipud(temp(2:end,2:end));
6
7 modelfun0 = @(b,x) b(1) + b(2)*cos(b(3)*x+b(4));
8
9 imax=10;
10 k=zeros(imax,1);
11
12 for i=1:imax
13
14     beta0 = [mean(d(i,:)), max(d(i,:))-min(d(i,:)), 2*pi/150, 0];
15
16     mdl0 = fitnlm(1:length(d),d(i,:),modelfun0,beta0);
17
18     k(i)=mdl0.Coefficients{3,1};
19
20 end
21
22 kavg = mean(k);
23
24 modelfun = @(b,x) b(1) + b(2)*cos(kavg*x+b(3));
25
26 framenum = min(size(d));
27 param=zeros(framenum,3);
```

```
28
29 for i=1:framenum
30
31     beta = [mean(d(i,:)), max(d(i,:))-min(d(i,:)), 0];
32
33     mdl= fitnlm(1:length(d),d(i,:),modelfun,beta);
34
35     param(i,:) =mdl.Coefficients {:,1};
36 end
37
38 x=1:length(d);
39 pks=zeros(framenum,10);
40 locs=zeros(framenum,10);
41
42 for i=1:framenum;
43
44     [pk,loc] = findpeaks(modelfun(param(i,:),x));
45
46     pks(i,1:length(pk))=pk;
47     locs(i,1:length(loc))=loc;
48 end
49
50 for i=10:-1:1
51     if sum(locs(:,i)) == 0
52         locs=locs(:,1:i-1);
53     end
54 end
55
56 simdata = xlsread('simulationdata.csv');
```



```
58 close all ;
59
60 sim808 = find(simdata<0.8686 & simdata>0.8684);
61 sim808x = simdata(sim808+length(simdata));
62 sim808y = simdata(sim808+2*length(simdata));
63
64 shift = 8;
65 sim808y(1:shift) = sim808y(1:shift) + 2*pi;
66 sim808y = circshift (sim808y,-shift);
67
68 a=diff( locs (:));
69 b=intersect( find(a<-10),find(a>-400));
70 yrepeat = round(mean(-1*a(b)));
71
72 c=diff(b);
73 c(c > 100) = [];
74 xrepeat = mean(c);
75
76 sim808x = sim808x * xrepeat/(2*pi);
77 sim808y = sim808y * yrepeat/(2*pi);
78 run(' eqline .m')
79
80 eqshift =shift+28;
81 eqy(1: eqshift) = eqy(1: eqshift) +pi;
82 eqy = circshift (eqy,[0,- eqshift]);
83 eqy=eqy-eqy(1,1);
84
85 eqx=eqx*xrepeat/pi;
86 eqx=eqx+sim808x(1,1);
87 eqy=eqy*yrepeat/pi;
```

```
88 eqy=eqy+sim808y(1,1);
89
90 hold on
91 for i=0:5
92     for j=0:3
93         %plot(sim808x+i*xrepeat,sim808y+j*yrepeat,'black')
94         plot(eqx+i*xrepeat,eqy+j*yrepeat,'black')
95     end
96 end
97
98
99 plot(locs,'black.')
100 hl = xlabel('Analyzer angle (\varphi) (rad)');
101 ylabel('Phase shift (\gamma_P) (rad)')
102
103 set(hl,'Interpreter','latex')
104 for i=0:7
105     xtickloc(i+1) = i*xrepeat;
106 end
107 set(gca,'XTick',xtickloc)
108 xticks = ['0 \pi'; '2\pi'; '3\pi'; '4\pi'; '5\pi'; '6\pi'; '7\pi'; '8\pi'];
109 set(gca,'XTickLabels',xticks)
110
111 for i=0:7
112     ytickloc(i+1) = i*yrepeat;
113 end
114 set(gca,'YTick',ytickloc)
115 yticks = ['0 \pi'; '2\pi'; '4\pi'; '6\pi'; '8\pi'];
116 set(gca,'YTickLabels',yticks)
117 hold off
```

Bibliography

- [1] R. Vyas and S. Singh, “Geometrical Phase of Light via Jones Matrices.” Unpublished (2014).
- [2] M. Berry, “The geometric phase,” *Scientific American* pp. 26–34 (1988).
- [3] S. Pancharatnam, “Generalized theory of interference.,” **A44**, 247 (1956).
- [4] W. Dultz and S. Klein, “Pancharatnam’s Phase in Polarization Optics,” *Advanced Electromagnetism: Foundations, Theory and Applications*, World Scientific (1995).
- [5] C. Welch and S. Singh, “Detecting Pancharatnam’s Phase using LG Vortex Beams,” (University of Arkansas 2015).
- [6] A. available at goo.gl/w27nYC.
- [7] B. Hils and W. Dultz, “Nonlinearity of Pancharatnam’s geometric phase in polarizing interferometers,” (1999).
- [8] J. Peatross and M. Ware, *Physics of Light and Optics* (2015 edition).

Index

Antipodal, 4

Pancharatnam's phase, 1

Polarization, 2

Polarization Circuit, 6

Solid Angle, 6